Composite Structures 160 (2017) 128–141

Contents lists available at ScienceDirect

Composite Structures

journal homepage: www.elsevier.com/locate/compstruct

Experimental and numerical failure analysis of notched quasi-unidirectional laminates at room temperature and elevated temperature

D. Flore [a,*], B. Stampfer [b], K. Wegener [a]

[a] Institute of Machine Tools and Manufacturing (IWF), ETH Zürich, Zurich, Switzerland
[b] Faculty of Mechanical Engineering, Karlsruhe Institute of Technology (KIT), Karlsruhe, Germany

ARTICLE INFO

Article history:
Received 22 April 2016
Revised 4 September 2016
Accepted 16 October 2016
Available online 17 October 2016

Keywords:
Quasi unidirectional/unbalanced fabric
Continuum Damage Mechanics
Notched laminates
Fracture toughness
Temperature impact

ABSTRACT

In this work an approach to predict the strength of notched structures made of quasi unidirectional glass fibre epoxy is presented. It takes into account the fabric specific behaviour in terms of hardening and softening. Four macroscopic ply failure modes are considered according to the Hashin criterion, depending on the direction of loading. Material hardening and softening is implemented according to Continuum Damage Mechanics. The hardening mechanism is modelled separately for matrix tension and shear. The softening mechanism is modelled by the incorporation of fracture toughness according to the failure mode (fibre/matrix failure in tension/compression). A new technique is proposed to determine the fracture toughness from uniaxial tension/compression tests of unidirectional notched laminate specimens. Special interest is given to the temperature impact on the material properties (elastic parameters, strengths and fracture energy) in a wide range (−40 °C to 160 °C). Since the interval covers the rubber temperature of epoxy the approach's reliability under such conditions is examined as well.

1. Introduction

The low specific weight of continuous fibre reinforced plastics (FRP) offers light weight design opportunities. Therefore, the application of FRP materials in automotive engineering is increasing since the year 2000, as shown by Lässig [1]. Carbon fibre composites approved well in lightweight structures. Glass fibre epoxy composites are candidates for cost sensitive applications due to low production cost. Unidirectional (UD) plies fail catastrophically at low stresses when loaded transversely to the fibre. This shortcoming is not present at balanced woven fabric. But their mechanical proprieties in warp and weft direction are reduced by towel crimp (undulation) which is described Puck [2]. As a result they reach low strengths, compared to fibre parallel loaded UD plies with the same fibre fraction. In quasi UD woven fabric towel crimp is less serious, which significantly improves their mechanical properties as described by Schürmann [3] and Karahan [4]. Quasi UD refers to strongly unbalanced fabric, where usually around 90% of fibres are aligned in warp direction. Quasi UD fabric combines the advantages of UD composites and balanced fabric: Good mechanical properties in fibre direction, a medium failure strain when loaded fibre transversely and a very high failure strain when loaded mainly by shear. This reduces the probability of catastrophic failure. To use the benefits of quasi UD glass fibre epoxy (GF-EP) fabric in structural application, a model is presented predicting the failure of notched structures under quasi-static loading. Since epoxy resin is sensitive to elevated temperatures, the model is validated for room and high temperatures. The influence of fibre volume fraction on the material properties is considered as well.

2. State of the art

2.1. Experimental

The mechanical behaviour of FRP is very different from metals since it is anisotropic and inhomogeneous. The failure of FRP is not determined by a single crack mechanism and its propagation but rather by several damage mechanisms. In the last years intense research revealed the failure phenomena of balanced, moderately unbalanced and quasi UD woven fabric.

Roy [5] examined unbalanced woven carbon fibre epoxy (CF-EP) fabric with a fibre ratio of 6:1 and compared it to a model laminate, which only contained crimp in warp direction. Lomov [6] examined triaxially woven and quasi UD fabric. The triaxial fabric is based on CF, placed longitudinally and in ±45° direction, which is

* Corresponding author.
E-mail address: Dominik.flore@gmx.de (D. Flore).

http://dx.doi.org/10.1016/j.compstruct.2016.10.046
0263-8223/

Nomenclature

Abbreviations

FRP	fibre reinforced plastics
CF	carbon fibre
GF	glass fibre
EP	epoxy
UD	unidirectional
MD	multidirectional
FVF	fibre volume fraction
CLT	Classical Laminate Theory

Symbols and parameters

φ	fibre volume fraction
T	temperature
σ	Cauchy stress
E	elastic Modulus
G	shear Modulus
H	hardening Modulus
r	material strength
D	damage parameter
G	fracture toughness
g	failure energy density
l	length

Indices

f	fibre
m	matrix
t	tension
c	compression
tan	tangent modulus
y	yield
0	initial ultimate
eq	equivalent
cri	critical
th	threshold
un	unnotched
FEM	Finite Element Method
CDM	Continuum Damage Mechanics
SR	stiffness reduction
RT	room temperature
HT	high temperature
E-Machine	Electric Machine
APDL	Ansys Parametric Design Language
ε	infinitesimal strain
υ	Poisson's ratio
C	stiffness
A	area
n	number
l	length
d	hole diameter
w	specimen width
F	specimen strength
Δ_{target}	optimization target
1	longitudinal to warp fibres
2	in ply transverse to warp fibres
3	out of ply transverse to warp fibres
El	element
IP	integration point
cra	crack
chr	characteristic
exp	experiment
sim	simulation
no	notched

embedded in EP. In the quasi UD fabric, not only the fibre ratio was strongly unbalanced, also the warp contained CF and the weft GF. Bonnafous [7] examined balanced hemp fibre epoxy fabric. Damage mechanisms were acoustically measured on component level and compared to acoustic emissions of the fabric. Daggumati [8] examined balanced fabric consisting of GF and a thermoplastic matrix. Damage initiation and progress were acoustically and visually measured. It revealed how the damage mechanism of a ply is influenced by its position in the laminate. Kergomard [9] examined the influence of crimping on damage mechanisms in quasi UD fabric, which consists of GF-EP with fibre ratio of 87:13. Kasrahan [4] examined the influence of fibre crimp on the mechanical ply properties of six fabrics types with an epoxy matrix. Carbon, Aramid and Glass fibres were used. The quasi UD fabric consists of a carbon fibre warp with a local fibre volume fraction (FVF) of 0.51 and a glass fibre weft. Kersani [10] examined quasi UD fabric consisting of flax and epoxy with a fibre ratio of 955:45. The beginning of failure in different laminate layups is acoustically measured and compared to the stress strain curves.

Even though structure and components of the examined fabrics vary, similar damage mechanisms occur. Damage progression in fabric generally is a multilevel phenomenon, it occurs on the microscale (fibre, matrix and interface), mesoscale (woven unit cell or ply level) and macroscale (laminate level).

According to Puck [2] the fabric failure mechanisms on the microscale are the same as in UD plies: In longitudinally loaded plies, single fibres break before the load reaches the ply strength. As described by Schürmann [3] and Talreja [11] this is caused by the statistical distribution of fibre defects. From this point, cracks either propagate along the fibre or load perpendicular into the matrix. As matrix cracks reach adjacent fibres and circumvent them, they cause fibre bridging. Nevertheless most fibres remain intact, explaining a nearly constant ply stiffness, until the load reached the ply strength. At the ply strength, fibre fracture accelerates causing ply stiffness degradation. Due to statistical distribution of the fibre strength and fibre pull out, cohesive behaviour is observed until final failure. In transversally loaded plies cracks nucleate at matrix flaws or fibre matrix interfaces (debonding). A single crack rapidly splits the (isolated) ply, growing load perpendicular within the matrix and along interfaces. The ply's stiffness remains constant until it fails in a brittle mode.

According to Lomov [6], Daggumati [8] and Bonnafous [7] the woven unit cell's failure phenomenology can be classified into certain stages:

- Damage initiation occurs in transversely loaded towels (microcracks) or at towel crossings (micro-delamination).
- Damage progression includes microcrack stopping at adjacent towels, crack propagation at towel crossings, and crack combination.
- The final failure mechanism is breakage of the towels in loading direction. This is to large extent driven by the separation of crossing towels through micro-delamination.

Lomov [6] observes a nonlinear stress strain curve for fibre inclined loaded quasi UD plies. The yield point corresponds to the occurrence of acoustically measured damage. The ply failure modes are similar to those of UD plies. Karahan [4] loads the quasi

UD ply by longitudinal tension. Thereby a moderates stiffening in the stress strain curve is observed. Kersani [10] observes a decrease of stiffness in the stress strain curve of longitudinally loaded quasi UD laminate. This is explained by the flax fibre intrinsic nonlinearity. The tension loaded [+45,−45] laminate shows a pronounced decrease in tangent modulus after circa a quarter of the failure strain.

2.2. Modelling

The failure analysis of FRP is generally a multiscale problem due to the inhomogeneous structure and multilevel failure mechanisms. Common levels of modelling are macroscopic (laminate), mesoscopic (fabric unit cell or ply level) or microscopic (constituent level). Macroscopic modelling means stress homogenization on laminate level. Such approach is rarely chosen nowadays, because modification might be required for each new laminate layup. Microscopic modelling is usually embedded in multiscale approaches, which model the interaction between microscale and mesoscale or macroscale. According to Aboudi [12] they are classified as hierarchic, synergistic or concurrent, depending on coupling of, and information transfer between the scales. A micromodel generally is a unit cell consisting of fibre, matrix and eventually an interface. Micro-modelling permits multiscale approaches to account for changes in unit cell composition in a physical way. Furthermore material failure is analysed in detail, because it is indicated on component level. A criterion with different cases for fibre and matrix failure is unnecessary. But modelling the interface and measuring the component properties remains a challenging task. Transferring properties from micro to meso-level is often based on the assumption of material periodicity. As soon as failure localizes in a ply, material periodicity cannot be guaranteed and the composite meso-structure becomes more important than the microstructure, as stated by Maimi [13]. Furthermore micro-modelling adds significant complexity to the material model and requires high computational resources. This is critical in the simulation of larger structures and in fatigue simulation, where static loading is calculated repetitively. Therefore modelling on ply level is preferred in this work.

Lomov [6] showed that for quasi UD fabric, on ply level, failure modes similar to UD plies can be distinguished. Failure including fracture of the warp equals fibre failure, failure including only fracture of the rare fibres in the weft equals matrix failure. Therefore a modified Hashin [14] criterion, developed to predict failure in UD plies, is used here. The criterion is used in its original two dimensional formulation, because the plies are assumed to be in a plain stress state. Interaction between the plies and the laminate is calculated using Puck's [2] Classical Laminate Theory (CLT).

Daggumati [8] and O'Higgins [15] examined stacking sequence effects. Changing the layup of a laminate can affect inter- or intralaminar failure mechanisms and thereby the laminate strength, even though the same plies are used. This is obviously caused by through-the-thickness-interaction of the plies. Since the CLT assumes plain stress and perfect sticking of the plies, stacking sequence effects are not modelled in this work.

As shown by Mollenhauer [16] the inhomogeneous stress field in notched laminates permits a strain redistribution. Embedded plies do not fail immediately but gradually, see e.g. Puck [2], Talreja [11] and Pinho [17]. In these cases it is crucial to not only model the material until it reaches the strength, but to include the failure process.

Techniques to predict the failure of open hole laminates being of analytical and phenomenological nature have been developed very early. Wadoups [18] applies Linear Elastic Fracture Mechanics by assuming the presence of an inherent flaw in FRP. The inherent flaw is a characteristic length of the composite which is added to the observable notch. Thereby the strength dependence on the hole radiusis predicted. Whitney [19] presents two approaches to indicate the failure of open hole laminates, the point stress and the averaged stress model. The point stress model predicts failure when the stress of the notched laminate at a certain distance from the hole exceeds the stress of the unnotched specimen. The average stress model predicts failure when the stress of the notched laminate, averaged over a certain distance from the hole, equals the average stress of the unnotched specimen. The approaches are fairly accurate for hole notched specimens, see Belmonte [20] and Camanho [21], but they include semi-empirical parameters which cannot directly be linked to physical mechanisms. Belmonte developed a critical damage growth model for GFRP [20] and CFRP [22] based on physical parameters. It is capable of predicting the failure of notched laminates, based on unnotched strength and fracture toughness. But the usage of laminate connected parameters requires new measurements for each notch form and laminate layup. Approaches which model the damage mechanisms on ply level are more versatile. Puck [2] states that embedded transversal plies in cross laminates do not fail completely when the load reaches the isolated ply strength. Rather they continue to bear load, which means that their stiffness is reduced gradually. Puck models this by reduction factors, which are the fraction of actual to initial elastic parameters. To account for a combined stress state the factors are given as a function of Puck's failure criteria factors. Kennedy [23] uses the reduction factors in the fatigue simulation of GF-EP quasi isotropic laminates. The reduction factor evolution of embedded plies is difficult to determine because it must be identified in laminate measurements. Measuring material softening in isolated plies is difficult as well, because the actual fracture process is limited to a narrow band where stress and strain are hardly measured, as stated by Krüger [24]. Coupling softening and (ply) fracture toughness is a widely used alternative to stress strain measurements. The coupling is established by assuming equality of the work, which is required to open a crack and dissipated energy, which is represented by the area under the stress strain curve of a material volume subjected to failure, see Harris [25] and Pinho [26]. In structural application the equivalence is often assumed for the total failure process, which makes the fracture toughness a material parameter. Considering the work energy equivalence in connection with the (areic) fracture toughness in FEM insures solution objectivity from the element size in localisation problems. It was firstly applied by Hillerborg [27] for the fracture of concrete. Maimi [13], Camanho [21] and Krüger [24] thereby predict the failure of notched FRP multidirectional (MD) laminates. Martin-Santos [42] presents a constitutive model for the simulation of fabric reinforced laminates. In contrast to the aforementioned authors he considers the shear nonlinearity. Isotropic, exponential hardening is implemented. As fibre tension material law, linear and a bilinear softening is considered. It turns out that bilinear softening provides a better prediction for the nominal strength of open hole specimens than linear softening.

Closely connected to material laws, which contain softening, is the identification of cohesive laws. Cohesive laws describe the relation between the stress and crack opening in the fracture process zone of quasibrittle materials such as FRP. A cohesive law can be transferred into a material law for finite element analysis, if the elements' dimensions are considered. Jacobsen [28] and Gregory [29] model fibre bridging in double cantilever beams. R-curves are measured and used to adjust the parameters of a cohesive law. In both cases different shapes were used and a piecewise defined law (linear softening followed by a power law softening) is found to fit experimental data best. Recently some effort has been made to experimentally obtain the softening law of laminates, which are modelled as one homogenised material. Zobeiry [38] conducted compact tension and compression tests and

determined the displacement field by digital image correlation. This data was used to estimate the size of the fracture process zone as well as the strains and stresses. Therefore no restriction on the shape of the material law is made in advance. Their conclusion is that for tension and also for compression, a trilinear material law (linear elasticity followed by bilinear softening) is sufficient to fit the specimen's load-pin displacement curve. Bergan [39] conducted compact tension tests and modelled them by assuming a cohesive trilinear law (linear elasticity followed by bilinear softening). The law's parameters were determined by two ways: The J-integral and the modified compliance method. The J-integral method requires to measure the strain by digital image correlation, creation of a FEM model and to integrate numerically around the crack tip, which causes some difficulties. The modified compliance calibration method is simpler to apply but relies on Linear Elastic Fracture Mechanics and is therefore less accurate for smaller specimens. Nevertheless both methods deliver similar cohesive laws. Furthermore Bergan [39] showed that similar cohesive laws are obtained for different specimen sizes. Thus the identified cohesive law can be seen as a material property. Ortega [40] as well conduct compact tension tests to identify the cohesive law of two types of laminates (glass fabric and glass carbon fabric). An inverse method is used to identify a piecewise linear law. The number of load-pin displacement points, used for calibration of the law, determines the number of segments. For the glass fabric laminate a trilinear softening law is found to be sufficient. For the glass carbon fabric laminate a five parameter law is suggested (piecewise constant stresses connected by an exponential decrease). Furthermore it is found that for open hole specimens the initial part of the softening law determines the nominal specimen strength. This conclusion was already drawn by Maimi [41], who examined the nominal strength of open hole laminates. Given the specimen geometry, the material strength and the cohesive law, the specimen strength is calculated analytically. Four softening shapes are examined: Constant, linear, exponential and bilinear. In fact the specimen strength is reached at small crack opening displacements, which explains the decisive role of the first part of the cohesive law. Thus the linear, the exponential and the bilinear laws are able to fit the specimen strength equally well.

In this work the failure process of notched GF-EP specimens is simulated by means of the Finite Element Method (FEM), which permits to analyse arbitrary geometries. In contrast to prevailing research quasi UD woven fabric, instead of UD composite, is considered. The material model accounts for pre failure nonlinearity in shear and weft direction. Until now FRP were rather modelled as linear elastic until the start of the failure process. Latter is here indicated by a modified Hashin criterion. For each ply failure mode a separate fracture toughness value is used. Different crack modi within one failure mode are not distinguished since Sanford [30] showed that the sum of toughness is constant for different crack modi in glass fibre reinforced plastics. By dividing the fracture toughness by a characteristic length the energy density is derived, which must be dissipated in the failure process of an integration point. The characteristic integration point length is chosen according to the crack band theory of Bažant and Oh [31]. After failure indication, further strain gradually reduces the elastic parameters, which are affected by the failure mode. Governing nonlinear material behaviour by stiffness reduction generally refers to Continuum Damage Mechanics (CDM). The final failure co-incidents with inability of the integration point to carry load. Modelling the failure process in literature is often restricted to room temperature. In this work an interval from low (−40 °C) to high temperatures (160 °C) is considered. As fracture toughness measurements generally require high effort, an alternative is proposed here: The values of the failure modi (fibre/matrix, tension/compression) are chosen to fit the strength of open hole laminates in uniaxial tension/compression tests.

3. Experimental data

Experimental investigations are performed on GFRP laminates with different layups. The matrix is a high-temperature epoxy-resin of low viscosity and consists of a resin component (EPIKOTE™ Resin 04434, HEXION™) and a hardener component (EPIKURE™ Curing Agent 04434, HEXION™). The reinforcing textile is a unidirectional plain weave (VR 434 GI96) with 90% of the fibres aligned in the main direction while 10% of them are woven transversally for stabilization. The overall fibre volume fraction of the different specimens is between 0.5 and 0.6. Resin transfer moulding is used for fabrication of the specimens. The last tempering step is at 160 °C to receive a glass transition temperature of the same value.

The resulting composite material is referred as "Bosch GFRP". To characterise the material parameters, tension and compression tests at unnotched specimens were performed. The stress strain curves are recorded by the measuring of force displacement curves and by dividing by the initial specimen area/lenght. Fig. 1 shows the experimental setup for tension and compression.

In compression tests no strain sensors are used, due to the short free specimen length. Instead the specimen strain was derived from the machine displacement. Specimen types and performed experiments are given in Table 1.

Fig. 2 shows the homogenized stress strain curve of tension and compression tests performed on the Type01 and Type05 specimen at RT.

The tension curves are linear until the beginning of failure where the curve becomes smoothly nonlinear. This can be explained by the gradual fibre fracture process. The hardly present pre-failure nonlinearity justifies a linear elastic modelling. A kneepoint that is sometimes seen in balanced fabric is not present. For the compression tests the absolute stress displacement curve is shown. The pre-failure behaviour is fairly linear.

Fig. 3 shows the homogenized stress strain curve of tension and compression tests performed on the Type02 and Type06 specimen at RT.

The specimens in tension show a pronounced kneepoint around a quarter of the failure strain. Further strain causes a stress increase with a tangent modulus of roughly the tenth part of the initial E Modulus. The kneepoint concurs with the occurrence of load transvers matrix microcracks in the test specimen. Even though each microcrack covers the crosssection, of the specimen, the weft fibres prevent it from fracture. Further strain steadily increases the number of microcracks. Cross laminates made of UD plies are well-known for analogous phenomena: After a kneepoint in the stress strain diagram of the specimen, microcracks occur within embedded, transversely loaded plies. The transverse hardening is modelled linear. For the compression test the absolute stress displacement curve is shown. The pre-failure behaviour is fairly linear.

Fig. 4 shows the homogenized stress strain curve of the tension tests performed on the Type04 specimen at RT.

The specimens show a pronounced nonlinear behaviour at one fifth of the failure strain. The tangent modulus of the following hardening is very low and decreases with further stain. The nonlinearity can only be attributed to shear hardening because the occurring weft stress in this test is lower than the kneepoint stress. Furthermore the failure strain is much higher than in the Type01 or Type02 specimen.

The tests leave the question whether the nonlinearity in transverse and shear direction is caused by stiffness reduction (damage) or plasticity. To answer this, cyclic tests on the Type02 and Type04

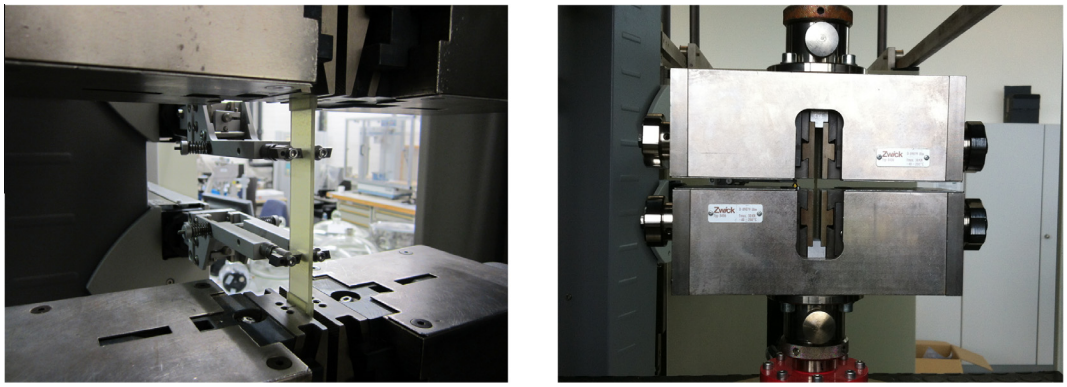

Fig. 1. Experimental setup for tension (left) and compression tests (right).

Table 1
Test conditions of unnotched specimen types used for material characterization.

Name	Layup	FVF	Temperatures [°C]	Test
Type01	$[0,0]_s$	0.41, 0.609	−40, 23, 160	Tension
Type05	$[0,0]_s$	0.609	23, 160	Compression
Type02	$[90,90]_s$	0.41, 0.525	−40, 23, 160	Tension, Cyclic
Type06	$[90,90]_s$	0.525	23, 160	Compression
Type04	$[-45,45]_s$	0.41, 0.57	−40, 23, 160	Tension, Cyclic (only RT)

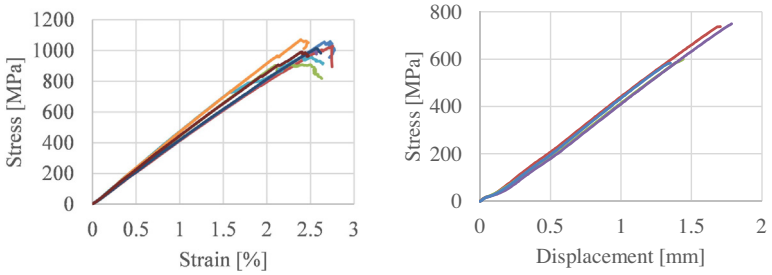

Fig. 2. Experimental stress strain curves of unnotched laminates under tensile (left) and compressive (right) longitudinal loading.

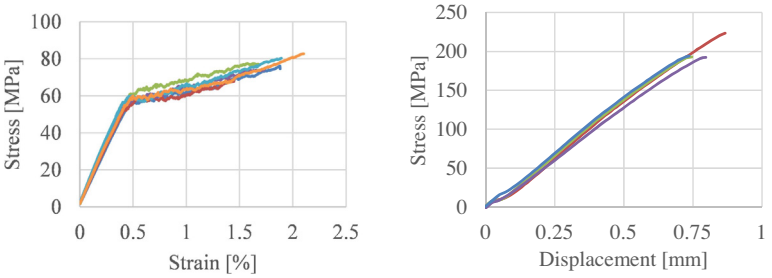

Fig. 3. Experimental stress strain curves of unnotched laminates under tensile (left) and compressive (right) transversal loading.

specimen are performed. Fig. 5 shows the corresponding stress strain curves.

The cyclic tests reveal that the nonlinearity is caused by both, damage and plasticity. In transverse tension the irreversible strain increases until a certain level, here around 0.1%, further cyclic loading decreases only the modulus. Increasing the strain amplitude in the shear laminate increases irreversible strain, while decreasing the modulus as well. For both specimens the same tendency is observed. At lower strains the irreversible strain (plasticity) is increased and the modulus is decreased as well (damage). Further strain decreases mainly the modulus, damage clearly predominates.

Ply stress and strain is generally considered in the natural coordinate system of a (quasi) UD ply: 1 indicates the warp or fibre direction (longitudinal), 2 the weft or matrix direction (transverse) and 3 the thickness direction. To characterise the Bosch GFRP in plain stress, tension and compression tests on unnotched Type01, Type02 and Type04 specimens are conducted for low, moderate and high temperatures. Specimens with a varying global FVF are also tested. This data permits to model the elastic material

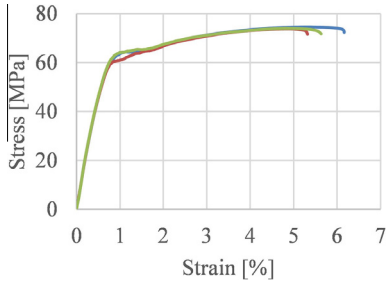

Fig. 4. Experimental stress strain curve of unnotched laminate under tensile diagonal loading.

parameters and strengths as a function of the temperature and the global FVF. The results for the longitudinal elastic modulus E_{11} and strength r_{11} are presented in Fig. 6.

The fitting is done by a polynomial, using FVF and temperature as variables and determining the parameters by the least squares method:

$$f(\varphi, T) = a + b \cdot \varphi + c \cdot T + d \cdot \varphi T + e \cdot T^2 \tag{1}$$

Temperature is inserted in °C, the FVF φ without unit. This approach was used for elastic parameters and (tension) strengths. Table 2 summarizes the polynomial parameters for the Bosch GFRP.

For shear the hardening modulus H_{12} is given, which is used in plasticity instead of the tangent modulus $G_{12,tan}$. In linear hardening the parameters are coupled via

$$G_{12,tan} = \frac{H_{12} \cdot G_{12}}{H_{12} + G_{12}} \tag{2}$$

The influence of temperature and FVF on the Poisson's ratio and compression strength is neglected. Therefore they are measured at RT and a medium FVF. The determined values are summarized in Table 3.

The out-of-plane Poisson's ratios ν_{13} and ν_{23} are used in simulation to calculate the normal strain in thickness direction.

4. Modelling

The material model in this work is implemented into the commercial FEM tool Ansys 14.5 via Ansys Parametric Design Language (APDL) and a usermat subroutine. The simulated laminates are modelled by SHELL181 elements. Each element contains multiple layers in thickness direction, which represent the laminate's plies and act together according to the CLT. Each layer contains a set of four integration points, which are equally spaced in the layer's midsurface. For the open hole specimens, which are presented in Section 4.4., free meshing was used in the area around the hole with a default edge length of 0.2 mm. The material modelling incorporates hardening, a failure criterion and softening. The fabric hardening in transversal tension and shear is actually a combination of plasticity and damage. However for reasons of simplification the hardening is modelled by damage only, which ensures an efficient and robust simulation. Assuming a plain stress state the components of the stiffness tensor in the natural coordinate system are modelled by

$$\begin{bmatrix} \sigma_{11} \\ \sigma_{22} \\ \sigma_{12} \end{bmatrix} = \begin{bmatrix} C_{1111} & C_{1122} & C_{1112} \\ C_{2211} & C_{2222} & C_{2212} \\ C_{1211} & C_{1222} & C_{1212} \end{bmatrix} \begin{bmatrix} \varepsilon_{11} \\ \varepsilon_{22} \\ \varepsilon_{12} \end{bmatrix} \tag{3}$$

$$C_{1111} = (1 - D_{11,s}) \frac{E_{11}}{X} \tag{4}$$

$$C_{2222} = (1 - d_{22,h})(1 - D_{22,s}) \frac{E_{11}}{X} \tag{5}$$

$$C_{1122} = C_{2211} = (1 - D_{11,s})(1 - D_{22,h})(1 - D_{22,s}) E_{22} \frac{\nu_{12}}{X} \tag{6}$$

$$X = 1 - \nu_{12}\nu_{21}(1 - D_{11,s})(1 - D_{22,h})(1 - D_{22,s}) \tag{7}$$

$$C_{1212} = 2(1 - D_{12,h})(1 - D_{12,s}) G_{12} \tag{8}$$

$$C_{1112} = C_{2212} = C_{1211} = C_{1222} = 0 \tag{9}$$

The evolution of the hardening parameters $D_{22,h}$ and $D_{12,h}$ for matrix tension and shear is outlined in Section 4.1. The evolution of the softening parameters $D_{11,s}$, $D_{22,s}$ and $D_{12,s}$ for fibre, matrix and shear is outlined in section 4.3. Similar models, which do not consider hardening damage, have been established by Matzenmiller [32] and Maimi [13].

4.1. Hardening

No interaction between hardening in transverse tension and shear is assumed. Since it is fairly linear in both cases a tangent modulus is used, $E_{22,tan}$ for matrix and $G_{12,tan}$ for shear hardening.

In transverse tension, hardening is indicated by a maximum stress criterion:

$$\sigma_{22} \geqslant r_{22,h} \tag{10}$$

The initial matrix hardening strength $r_{22,h}$ is the experimental matrix yield strength $r_{22,y}$. In case of hardening, $r_{22,h}$ is updated by the newly calculated matrix normal stress. The matrix hardening damage $D_{m,h}$ is calculated by Eq. (11), while $\varepsilon_{22,y}$ being the yield point strain.

$$D_{m,h} = 1 - \frac{E_{22,tan}}{E_{22}} + \frac{E_{22,tan}}{E_{22}} \cdot \frac{\varepsilon_{22,y}}{\max(\varepsilon_{22})} - \frac{\varepsilon_{22,y}}{\max(\varepsilon_{22})} \tag{11}$$

The matrix hardening parameter in the stiffness tensor is chosen according to the sign of the matrix stress.

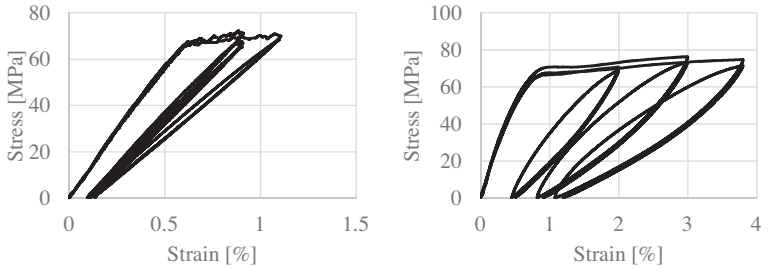

Fig. 5. Material response under cyclic loading for transverse tension (Type02, left) and fibre diagonal tension (Type04, right).

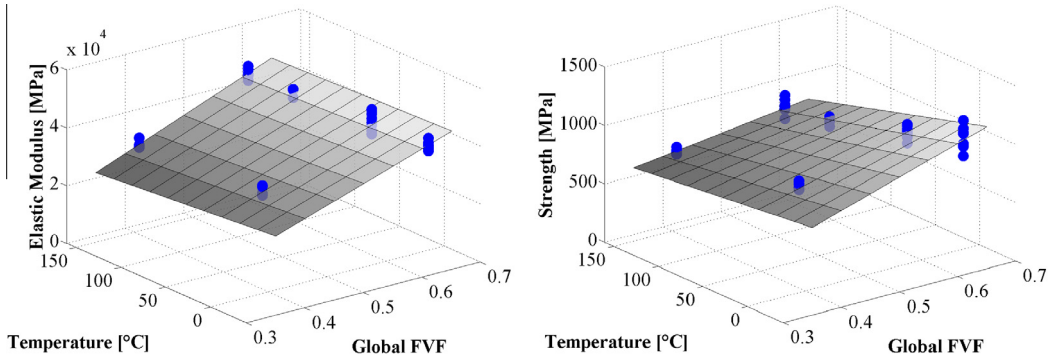

Fig. 6. Fit of E Modulus and strength, based on experimental results of unnotched Type01 specimens.

Table 2
Polynomial parameters to fit the Bosch GFRP in dependence of temperature and FVF.

Material parameter [MPa]	*a*	*b*	*c*	*d*	*e*
E_{11}	1575.243	70342.666	−47.469	55.667	0
$r_{11,t,0}$	230.961	1375.571	0.709	−4.553	0
E_{22}	−5024.628	35674.026	73.718	−178.343	−0.219
$E_{22,tan}$	−2132.021	6937.132	16.919	−35.401	−0.008
$r_{22,y}$	56.879	2.327	−0.091	0.025	0
$r_{22,t,0}$	−10.974	174.521	0.489	−1.141	0
G_{12}	−2444.473	11732.656	1.375	−38.902	0
H_{12}	−798.373	1874.313	−1.438	1.242	0
$r_{12,y}$	−73.86	201.5	0.195	−0.644	0
$r_{12,0}$	−16.448	129.452	−0.009	−0.312	0

Table 3
Material parameters of the Bosch GFRP not fitted to temperature and FVF.

$r_{11,c,0}$ [MPa]	$r_{22,c,0}$ [MPa]	ν_{12}	ν_{13}	ν_{23}
667	200	0.31	0.35	0.4

$$D_{22,h} = \begin{cases} D_{m,h}; \sigma_{22} > 0 \\ 0; \sigma_{22} \leqslant 0 \end{cases} \tag{12}$$

Shear hardening is calculated analogous, apart from using the absolute shear stress. Since is not distinguished between positive and negative shear, shear hardening parameter in the stiffness tensor $D_{12,h}$ always equals the shear hardening damage. Matrix hardening only occurs as long as matrix failure has not been active, shear hardening only as long as fibre tension, matrix tension and matrix compression failure has not occurred.

4.2. Failure criteria

Our experiments confirm the findings of Lomov [6]: The ply failure modes of quasi UD fabric are analogue to UD FRP. Wei [33] successfully used the Hashin criterion [14] even for balanced fabric. Therefore the Hashin criterion is chosen here to indicate start of the failure process. Fibre or matrix mode in tension or compression is distinguished. In contrast to the original criterion, fibre tension failure is only predicted when fibre stress exceeds half of the fibre tension strength. It insures that fibre failure is always driven by fibre tension, because shear stress driven fibre failure was not observed in experiments. The threshold value is chosen this way, because Schürmann [3] states that fibre fracture starts as longitudinal tension reaches half of the ply strength.

Fibre tension failure $\sigma_{11} > 0.5 r_{11,t}$

$$\left(\frac{\sigma_{11}}{r_{11,t,0}}\right)^2 + \left(\frac{\sigma_{12}}{r_{12,0}}\right)^2 = 1 \tag{13}$$

Fibre compression failure $\sigma_{11} \leqslant 0$

$$\left(\frac{\sigma_{11}}{r_{11,c,0}}\right)^2 = 1 \tag{14}$$

Matrix tension failure $\sigma_{22} > 0$

$$\left(\frac{\sigma_{22}}{r_{22,t,0}}\right)^2 + \left(\frac{\sigma_{12}}{r_{12,0}}\right)^2 = 1 \tag{15}$$

Matrix compression failure $\sigma_{22} > 0$

$$\left(\frac{\sigma_{22}}{r_{22,c,0}}\right)^2 + \left(\frac{\sigma_{12}}{r_{12,0}}\right)^2 = 1 \tag{16}$$

The simplified matrix compression failure criterion is used, because experiments indicated that two times the shear strength $2r_{23,0}$ fairly equals the transversal strength $r_{22,c,0}$. The same simplification is also used by Shokrieh [34].

4.3. Softening

Fracture toughness is included to the FEM simulation by the Crack Band Theory [31]. The main idea is that the failure process localises in the smallest unit of calculation due to softening. Therefore the fracture energy in FEM must be dissipated on integration point level, which requires a quantity of the unit energy density. The energy density is calculated by dividing the physical fracture toughness of the failure mode by a numerical characteristic length.

$$g = \frac{G}{l_{chr}} \tag{17}$$

The characteristic length generally is connected to one integration point (IP), where the FEM calculates stresses and strains. It is assumed, that the IPs are equally spaced in the two dimensional elements. Therefore the area connected to one IP is calculated as $A_{IP} = A_{El}/n_{IP}$. The mean "IP edge length" of a quadrilateral element

is calculated as $l_{IP} = \sqrt{A_{IP}}$. This is a good estimation, as long as the element shape is close to a square. Generally it must be considered that the fracture plane is placed arbitrary in the element area. In this case the crack and IP length are coupled via projection.

$$l_{cra} = \frac{l_{IP}}{\cos(\phi)} \tag{18}$$

ϕ is the inclination between crack and IP edge, the maximum is $\pi/4$. To account for this in the mean, the characteristic length is calculated as

$$l_{chr} = \frac{4}{\pi}\int_0^{\frac{\pi}{4}} l_{cra}\, d\phi = 1.12\sqrt{\frac{A_{El}}{n_{IP}}} \tag{19}$$

Considering this the characteristic length in triangular elements is $1.52\sqrt{\frac{A_{El}}{n_{IP}}}$, according to Maimi [35].

The validity of a criterion for a certain failure mode marks the beginning of the material softening, similar to Puck's reduction factor approach [2]. While softening, the shape of the stress strain curve can be linear, progressive (above linear), regressive (below linear) or multilinear. Maimi [35] and Krüger [24] use a regressive evolution, except for fibre tension where softening initially evolves linear. A progressive softening evolution can be found in Matzenmiller [32]. Pinho [17] use linear softening to model the degradation of embedded plies. As outlined in the literature review, recently some effort has been done to obtain the cohesive law in laminates. A bilinear softening law appears appropriate to describe most of the experiments. Nevertheless linear softening is used here. In this case softening damage generally evolves according to the following equations, derived from Ansys [36].

$$D = \frac{\varepsilon_{eq}^{cri}}{\varepsilon_{eq}^{th}} \cdot \frac{(\varepsilon_{eq}^{th} - \varepsilon_{eq}^{0})}{\varepsilon_{eq}^{cri} - \varepsilon_{eq}^{0}} \tag{20}$$

When the Hashin criterion is fulfilled for a certain failure mode, the initial equivalent strain ε_{eq}^{0} and the threshold strain ε_{eq}^{th} are set to the current equivalent strain: $\varepsilon_{eq}^{0} = \varepsilon_{eq}^{th} = \varepsilon_{eq}$. The critical equivalent strain ε_{eq}^{cri} is calculated as

$$\varepsilon_{eq}^{cri} = \frac{2 \cdot g}{\sigma_{eq}} \tag{21}$$

The equivalent stress σ_{eq} and the equivalent strain ε_{eq} are calculated according to the particular failure mode. Here denotes the McCauley brackets which gives the term in brackets, if it is positive and otherwise zero.

Fibre tension failure

$$\varepsilon_{eq,ft} = \sqrt{\langle\varepsilon_{11}\rangle^2 + 2\varepsilon_{12}^2} \tag{22}$$

$$\sigma_{eq,ft} = \frac{\langle\sigma_{11}\rangle\langle\varepsilon_{11}\rangle + \sigma_{12}2\varepsilon_{12}}{\varepsilon_{eq,ft}} \tag{23}$$

Fibre compression failure

$$\varepsilon_{eq,fc} = -\langle\varepsilon_{11}\rangle \tag{24}$$

$$\sigma_{eq,ft} = -\langle\sigma_{11}\rangle \tag{25}$$

Matrix tension failure

$$\varepsilon_{eq,mt} = \sqrt{\langle\varepsilon_{22}\rangle^2 + 2\varepsilon_{12}^2} \tag{26}$$

$$\sigma_{eq,ft} = \frac{\langle\sigma_{22}\rangle\langle\varepsilon_{22}\rangle + \sigma_{12}2\varepsilon_{12}}{\varepsilon_{eq,mt}} \tag{27}$$

Matrix compression failure

$$\varepsilon_{eq,mc} = \sqrt{\langle-\varepsilon_{22}\rangle^2 + 2\varepsilon_{12}^2} \tag{28}$$

$$\sigma_{eq,ft} = \frac{\langle-\sigma_{22}\rangle - \langle\varepsilon_{22}\rangle + \sigma_{12}2\varepsilon_{12}}{\varepsilon_{eq,mc}} \tag{29}$$

The equivalent strain is calculated continuously. If it exceeds the threshold strain, the threshold is updated and damage increased until it reached a maximum of 0.9999. A positive damage rate insures the fulfilment of the second law of thermodynamics, for details see Maimi [13]. The so calculated fibre/matrix tension/compression damage variables D_{ft}, D_{fc}, D_{mt} and D_{mc} are incorporated to the stiffness according to the sign of fibre and matrix stress.

$$D_{11,s} = \begin{cases} D_{ft}; \sigma_{11} > 0 \\ D_{fc}; \sigma_{11} \leqslant 0 \end{cases} \tag{30}$$

$$D_{22,s} = \begin{cases} D_{mt}; \sigma_{22} > 0 \\ D_{mc}; \sigma_{22} \leqslant 0 \end{cases} \tag{31}$$

The shear damage is calculated as maximum damage of these failure modes. This is a difference to Ansys [36] where the shear damage is calculated by multiplying the damage variables. Thus the shear modulus will be damaged twice if damage in fibre tension and matrix tension is present. However a double amount of shear damage in such case could not be verified by experiments and therefore the following equation is used.

$$D_{12,s} = \max(D_{ft}, D_{fc}, D_{mt}, D_{mc}) \tag{32}$$

A multiple/parallel shear degradation by more than one failure mode is thereby neglected.

4.4. Calibration process for fracture energy

The material parameters derived so far allow simulation of unnotched specimens. The failure process occurring in notched specimens differs because the inhomogeneous stress strain state permits stress strain redistribution. To examine this, notched specimens were tested, whose geometry is presented in Fig. 7.

Apart from the hole, the specimen geometry is the same as the unnotched plies. Two diameters were tested for most specimen types with a diameter to width ratio (d/w) of 0.1 or 0.3, to gain comprehensive data. The hole diameter in UD laminates is 1 mm or 3 mm, the diameter in MD laminates 2 mm or 6 mm.

In Fig. 8 the measured relative specimen strengths are compared to results from literature obtained with other composites. Here r_{no} is the strength of the notched specimen and r_{un} is the strength of the unnotched specimen. For both, notched and unnotched specimens, the gross cross section is considered.

Thus the straight dashed line refers to a material which is completely insensitive to notches while the dotted line refers to a hole-sensitive material. This quite common representation can also be found in Lee [37]. The Bosch GFRP in some experiments even lies above this line. The phaenomena that notched FRP laminates sometimes reach higher relative strengths in static tension, or residual strengths after fatigue loading than unnotched laminates, is referred to as notch paradoxon, see e.g. Waddoups [18]. In terms of relative strength the Bosch quasi UD GFRP performs very well compared to balanced woven GF-EP [20], balanced woven CF-EP [22], UD GF-EP [15] and UD CF-EP [15,21].

First approaches to predict the strength of notched laminate by FEM simulation included linear elasticity until failure and a classical stiffness reduction approach: The elastic parameters are fully degraded according to the failure mode indicated by the Hashin

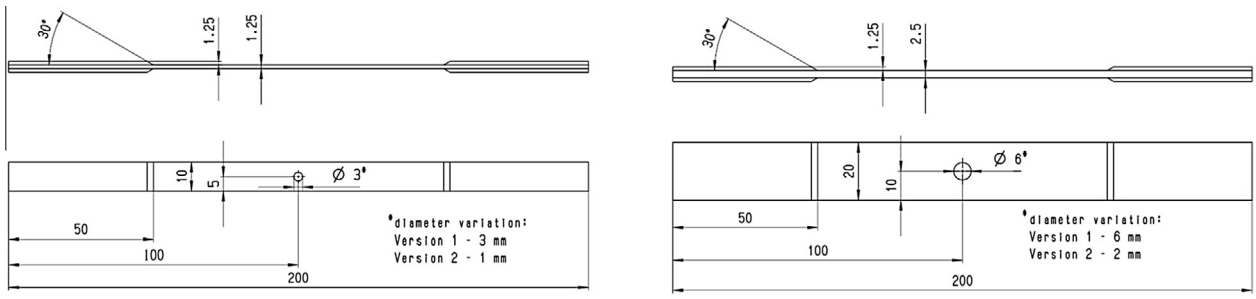

Fig. 7. Geometry of notched UD laminate (left) and MD laminate (right) specimens.

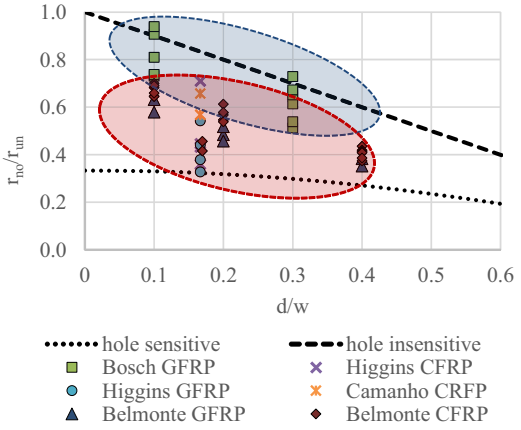

Fig. 8. Comparison of relative specimen strength of opden hole laminates, Bosch GFRP vs. literature G_{mc}.

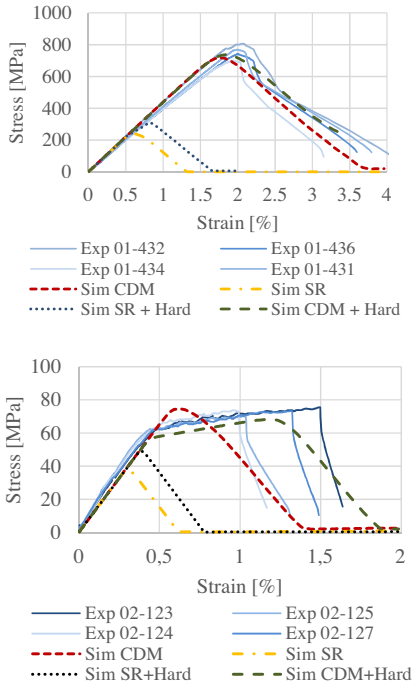

Fig. 9. Influence of fracture toughness on notched laminate (d/w = 0.1) simulation in longitudinal tension (Type01, left) and transvers tension (Type02, right).

criterion. The simulated specimen strengths turned out to be in the zone of hole-sensitive, brittle materials, indicated in Fig. 8, and thus far below experiments. An example is given in Fig. 9 by the curves 'Sim SR'.

Including weft and shear hardening increases the simulated strength, which is illustrated by the curves 'Sim SR + Hard' in Fig. 9. In longitudinal tension the material mainly fails due to warp tension. Thus weft and shear hardening contribute little to the specimen strength and it remains far below the experimental data. In transverse tension the material mainly fails due to weft tension. Thus hardening significantly raises the specimen strength. However it clearly remains lower than the experimental one and the curve shapes diverge.

Realistic specimen strengths are simulated only after the incorporation of softening by CDM ('Sim CDM'). By defining the IP failure energy density the fracture toughness governs the stiffness degradation. A slower softening counters localization and permits continuous stress strain redistribution to undamaged IPs. Thus it raises the specimen strength, compared to the stiffness reduction approach, which causes a sudden localization. The fracture toughness values were not determined experimentally but fitted to certain experiments. The process is outlined below.

Incorporating hardening to CDM simulations marginally adjusts the strength ('Sim CDM + Hard'). Rather it alters the stress strain curve shape in tests where hardening is clearly present, which can be seen in Fig. 9, right. It might be interesting to note that hardening only alters the stress strain curve when softening is incorporated as well. An explanation is that including softening spreads the failure process. This causes many elements to harden parallel, thus the individual hardening curve is observable on specimen level.

The fracture toughness values were not measured traditionally. Instead they were determined to fit the strength of the notched UD laminates with two hole diameters, which can be seen in Fig. 10 on the left. These simulations are sensitive to fibre tension, matrix tension and matrix compression fracture toughness. The failure modes occur despite longitudinal/transversal specimen loading due to the hole induced inhomogeneous stress state.

The minimised target value is the sum of squared relative specimen strength differences of experiment and simulation. The experimental strength of specimen i is denoted by $F_{exp,i}$, the simulated strength by $F_{sim,i}$. $i = 1$ refers to Type01 and $i = 2$ to Type02.

$$\Delta_{target} = \sum_{i=1}^{2} \left(\frac{F_{exp,i,d=1} - F_{sim,i,d=1}}{F_{exp,i,d=1}} \right)^2 + \left(\frac{F_{exp,i,d=3} - F_{sim,i,d=3}}{F_{exp,i,d=3}} \right)^2 \quad (33)$$

Both diameters $d = 1$ and $d = 3$ are considered because using only one diameter and therefore two specimens would not allow determining three toughness values. The aforementioned simulations are not sensitive to fibre compression toughness G_{fc}. This value is therefore chosen to fit the compression strength of a notched laminate in longitudinal loading. The thereby determined fracture toughness values are given in Table 4.

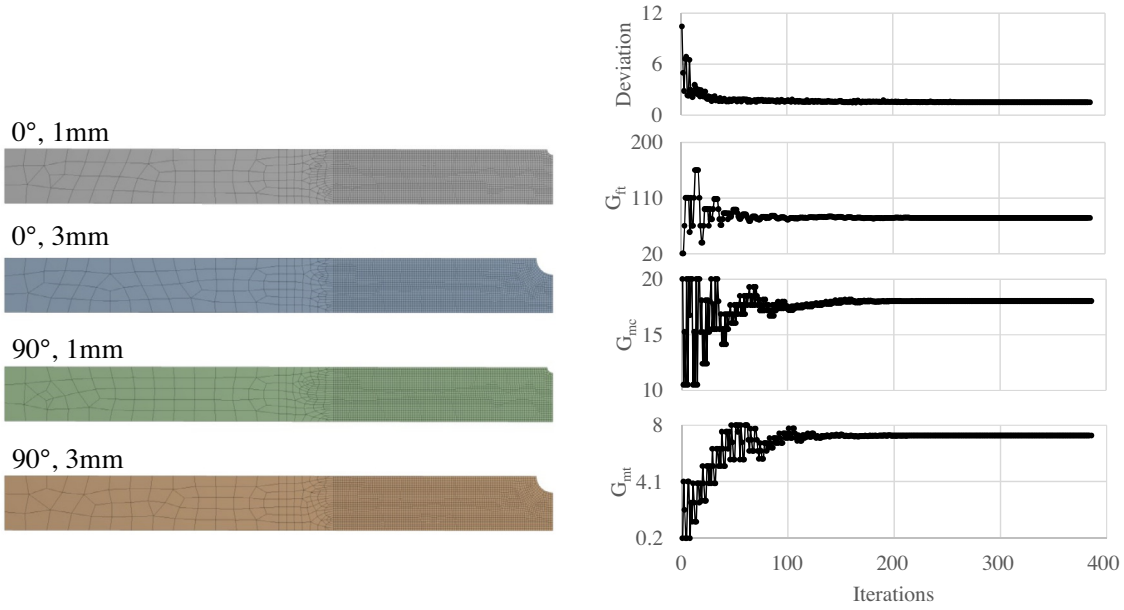

Fig. 10. Multi-target optimization: Used simulations (Type01/02, d = 1/3 mm, left), convergence diagram of fracture toughness values G_{ft}, G_{mt} and (right).

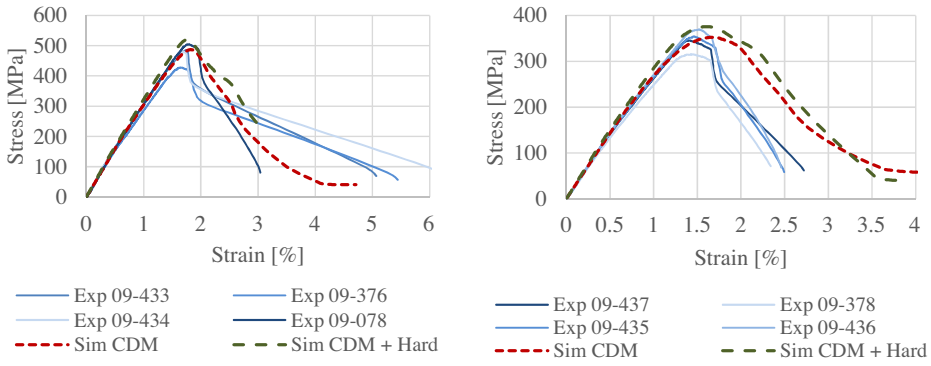

Fig. 11. Notched laminate Type09, tensional loading: Experiments and Simulation with d = 2 mm (left) and d = 6 mm (right).

To summarize the results, experimental and simulated strengths of calibrated specimens are given in Table 5

The UD specimen types to calibrate fracture toughness values are not unambiguous. It is also conceivable to determine the values by means of four hole notched UD laminates having one diameter, each loaded longitudinal/transverse in tension/compression. But the main idea is, that the exact specimen geometry is not decisive, as long it is significant to the desired fracture toughness value. Irrespective of the used UD laminates the proceeding has certain advantages compared to traditional fracture toughness measurements. Introducing an open hole into a UD laminate is much simpler than introducing a sharp crack to a fracture toughness specimen. Ordinary tension and compression tests can be conducted quick and easy, compared to traditional compact tension and compression tests. Especially when the orthotropic material behaviour is considered, evaluation of the traditional tests takes much effort, see e.g. Pinho [26], who numerically calculates the J-Integral in dependence of the crack length.

Some remarks follow, which consider the calibration process. Open hole UD laminates often fail due to ply splitting when loaded longitudinally and not due to fibre failure. This behaviour would prohibit an accurate calibration of the fibre tension fracture toughness. In this case another specimen geometry must be chosen, in which significant fibre failure occurs. For the Bosch GFRP we do not see significant ply splitting in the open hole specimen. An example is given in Fig. 12. As outlined in the literature review, another point concerning the open hole specimen is, that the ultimate load (the point used to adjust the fracture toughness) is often reached well before the cohesive law is exhausted at any point of the specimen. Calibrating the fracture toughness to the specimen strength could therefore cause an error. With the Bosch GFRP, the specimen stress curve is met fairly well, also after the ultimate load, where the fibre damage variable reaches one in many integration points. This implies that the fracture toughness error is acceptable. If there was significant deviation from the experiment at decreasing specimen stress, the problem could be solved by calibrating the fracture toughness not only to the ultimate stress, but also to stresses, which appear later in the curve. In cases where

Table 4
Fracture toughness values derived by notched UD laminate multi-target optimization.

G_{ft} [kJ/m^2]	G_{fc} [kJ/m^2]	G_{mt} [kJ/m^2]	G_{mc}[kJ/m^2]
78.06	17.97	7.23	60

Table 5
Comparison of experimental and simulated specimen strengths after fracture toughness calibration.

	Type01, d = 1 mm	Type01, d = 3 mm	Type02, d = 1 mm	Type02, d = 3 mm	Type05, d = 1 mm	Type05, d = 3 mm
F_{exp} [MPa]	754.1	528.5	73.1	57.1	540.4	435.1
F_{sim} [MPa]	716.0	465.0	74.6	56.7	606.9	464.8
Failure [%]	−5.05	−12.02	2.01	−0.66	12.31	6.48

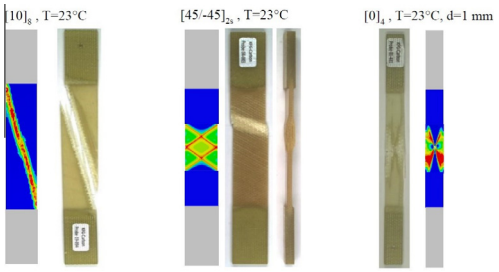

Fig. 12. Spatial damage evolution in unnotched and notched laminates under tensional loading: D_{mt} (left), D_{mt} (middle) and D_{ft} (right).

the agreement between simulation and experiment is still not satisfying, a bilinear softening approach could be used.

5. Results

It is of great importance that the fracture toughness values derived by notched UD laminate calibration are generally applicable. Therefore results of UD and MD laminates not used for calibration and an E-Machine rotor structure are presented in this chapter to validate the CDM model as well as the new calibration method.

5.1. Notched laminate

The validation on specimen level is performed using various layups and hole diameters. The notched laminates used for validation are summarized in Table 6.

The stress strain curves of the notched Type09 laminate with diameters of 2 and 6 mm loaded in tension are presented in Fig. 11.

The stress strain curves in simulation and experiments show some difference in the failure process, but the laminate strengths agree well for simulations independent of hardening incorporation. In the following hardening is neglected because the main goal of this work is the prediction of the ultimate stresses. If the shape of the stress strain curve was considered, modelling of hardening would be important, in cases where hardening is visible on specimen level. An example is the tensional loading of the notched Type02 specimen that can be seen in Fig. 9.

The comprehensive data of notched laminate strengths tested for validation at RT is given in Table 7.

Three to five tests were conducted for each laminate type. The presented laminate strength is the mean value. The results agree well for the Type06, Type09 and Type17 specimen. Especially the hole diameter has small influence on the agreement. This emphasises that the fracture toughness is a material parameter. The Type03 simulation exceeds the experimental strength by more than 10%. The laminate consists of [10,−10] plies. Simulation of the unnotched laminate with the Hashin criterion overestimates the experimental strength by 6.6%. This indicates that the failure is at least partly caused by the Hashin criterion and not by the fracture toughness. Thus it is assumed that the simulation accuracy could be improved by a better modelling of the transition between fibre and matrix failure mode at small fibre load inclination. Simulation of the Type07 (cross) laminate underestimates the experimental strength by almost 30%. The unnotched laminate strength is not reached in simulation as well, with 9% the failure is significant. Additionally a strong stacking sequence effect is observed in cross laminates: If plies of the same kind are blocked together, as apparent in Type07, laminate is notch insensitive and the notched strength is high. If the stacking is changed to an alternating sequence the laminate is notch sensitive and the notched strength is low, see O'Higgins [15]. The fracture toughness can not incorporate such effect, because it was calibrated at UD specimens. Neglecting stacking sequence and through-thickness effects is a general problem of plane stress ply modelling. Approaches to model stacking sequence effects anyway, e.g. by adapting the ply strength according to its position in the laminate, are presented by Camanho [21] and Pinho [17].

By FEM simulation it is not only possible to calculate the ultimate stress or stress strain curves, but to predict the spatial damage evolution as well. An example of this is given in Fig. 12.

Table 6
Notched laminates used for validation.

Type	Layup	Hole d [mm]	φ	T [°C]	Load
Type01	$[0/0]_s$	1, 3	0.609	160	Tension
Type02	$[90/90]_s$	1, 3	0.525	160	Tension
Type03	$[10/-10/10/-10]_s$	2, 6	0.566	23	Tension
Type06	$[90/90]_s$	1, 3	0.517	23	Compression
Type07	$[0/0/90/90]_s$	6	0.6	23	Tension
Type09	$[0/90/10/-10]_s$	2, 6	0.578	23	Tension
Type17	$[60/-60/20/-20/\underline{0}]_s$	6	0.6	23	Tension

Table 7
Strength comparison of notched laminates tested for validation at RT.

	Type03, d = 2 mm	Type03, d = 6 mm	Type06, d = 1 mm	Type06, d = 3 mm	Type07, d = 6 mm	Type09, d = 2 mm	Type09, d = 6 mm	Type17, d = 6 mm
F_{exp} [MPa]	595.8	434.0	188.6	135.1	334.5	474.2	346.0	252.7
F_{sim} [MPa]	658.9	503.8	184.0	139.0	239.2	486.3	352.2	258.5
Failure [%]	10.45	15.89	−2.42	2.9	−28.56	2.5	1.73	2.08

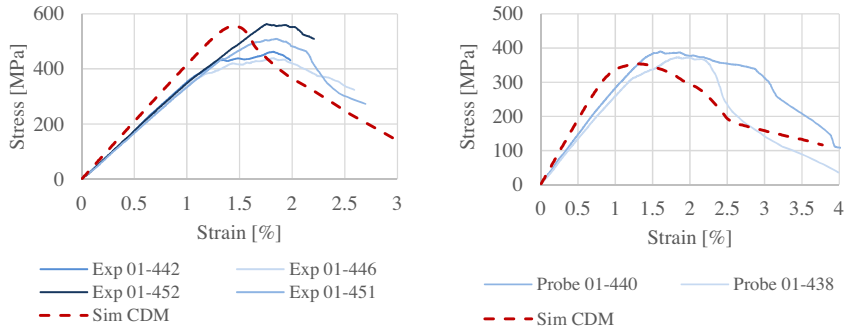

Fig. 13. Notched laminate, HT simulation: Tensional loading of Type01 laminate for d = 1 mm (left) and d = 3 mm (right) at T = 160 °C.

The unnotched $[10]_8$ laminate obviously fails by matrix tension mode and therefore the matrix tension damage parameter is shown. The damage evolves along the fibre. The matrix tension damage parameter is also shown in the unnotched $[45,-45]_{2s}$ laminate. Since the laminate is symmetric the simulation predicts a symmetric damage field. In fact the specimen always has imperfection which causes an asymmetric damage field. Still it can be seen that the damage evolves along the fibre in simulation and experiment. The fibre tension damage parameter is shown in the notched laminate $[0]_4$. The damage evolves cross like from the notch to the specimen edges. This is predicted fairly well by the simulation.

High temperatures are often critical in FRP, because polymers are usually temperature sensitive. The resin material behaviour changes significantly when it reaches the rubber temperature. Since high temperatures can not be excluded in some applications, it is of interest how the simulation behaves in this case. Fig. 13 shows the stress strain curves of the notched Type01 specimen.

For the influence of temperature on the fracture toughness some considerations must be made in advance. The calibration process for the fracture toughness resulted in G_{ft} = 78.06 kJ/m^2 and G_{mt} 7.23 kJ/m^2. In fibre direction the Bosch GFRP has a fibre volume fraction of 0.54 and in the transverse direction the fibre volume fraction is about 0.06. This pair of values is presented in Fig. 14. It can be seen that the fracture toughness is increased by increasing the fibre volume fraction in the loading direction. Having no fibres in the transverse direction the fracture toughness is about 0.27 kJ/m^2 according to Camanho [21]. Even though it is well-known that fracture toughness results from the interaction of fibre, matrix and interface, we here assume that the fracture toughness is mainly influenced by the fibres. Their properties however are hardly influenced by temperatures around 160 °C. Thus the fracture toughness values, calibrated at room temperature, are held constant at high temperatures.

All the other parameters are calculated using Eq. (1). Due to the polynomial approach, experimental and simulated elastic modulus differs. Apart from this the stress strain curve prediction in Fig. 13 is fairly good for both diameters. The specimen strengths for the notched UD laminates in transverse and longitudinal tension at 160 °C in experiment and CDM simulation are given in Table 8.

The simulated specimen strengths deviate from the experimental data by 8–16%. Still the accuracy is good, considering the large temperature difference of 137 K. If the fracture toughness was governed by the epoxy matrix, much higher deviations would be expected. It follows that mainly fibres influence the fracture toughness in the matrix tension and fibre tension failure mode. This justifies neglecting fracture toughness adjustment in many applications.

5.2. Structure

Another advantage of the FEM is the ability of calculating arbitrary geometries and notch shapes. Only this permits to predict the failure in complex structures. Hence a sector of an E-Machine rotor is simulated to validate FEM and CDM coupling and the fracture toughness calibration. The task of the rotor is to carry magnets and to transform the magnetic force into a driving torque. The main loading is caused by centrifugal forces. The rotor has a quasi-isotropic stacking of 24 layers whereat each layer is rotated

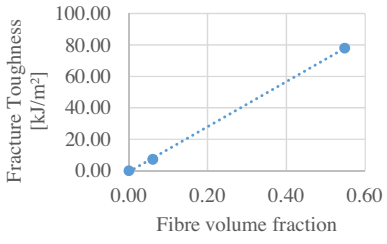

Fig. 14. Relation between fracture toughness and fibre volume fraction.

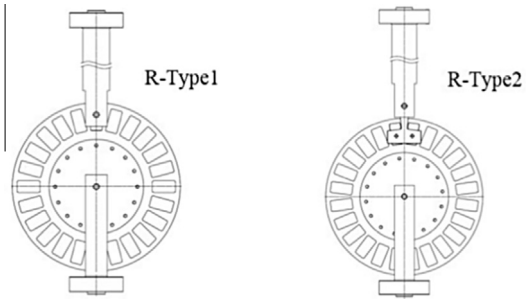

Fig. 15. Two different testing setups for the rotor disc.

Table 8
Strength comparison of notched laminates tested for validation at HT.

	Type01, d = 1 mm, HT	Type01, d = 3 mm, HT	Type02, d = 1 mm, HT	Type02, d = 3 mm, HT
F_{exp} [MPa]	493.4	381.5	51.5	41.4
F_{sim} [MPa]	555.63	353.39	59.56	45
Failure [%]	12.61	−7.37	15.66	8.57

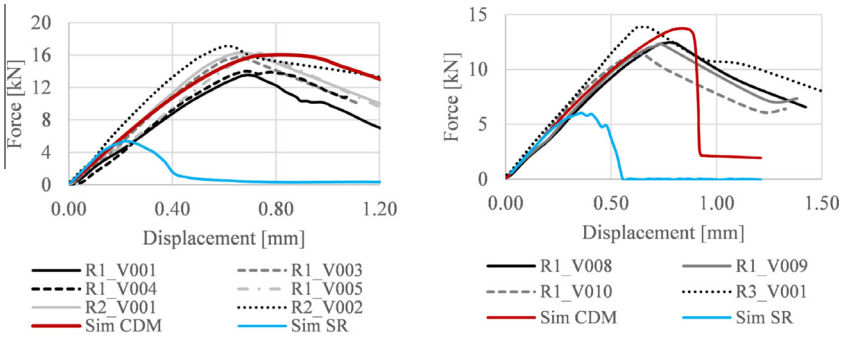

Fig. 16. Rotor structure: Force displacement curve for R-Type1 and R-Type2.

15° to its neighbour layer. Furthermore the rotor has symmetrical layup. Two different setups are tested that can be seen from Fig. 15. In the first, tension is applied via one magnet on the rotor segments (R-Type1), in the second via two magnets (R-Type2).

The simulation of the quasi-static loading is done using the CDM model without hardening and also using the stiffness reduction model. Fig. 16 compares force displacement curves in experiment and simulation.

Again a stiffness reduction approach drastically underestimates the maximum force, incorporation of CDM leads to realistic values. Since four layered UD laminates were used for calibration, whereas the rotor consists of 24 layers, the good results in terms of maximum force confirm that the derived fracture toughness values can be regarded as material parameters. The simulated (CDM) force displacement curve of R-Type1 agrees well with experiments. The sudden drop after maximum force in the R-Type2 CDM simulation curve is not seen in experiments and requires further examination. The experimental fracture pattern is compared to the damage evolution simulated by the CDM approach. The results of R-Type1 are given in Fig. 17, those of R-Type2 in Fig. 18.

The spatial damage evolution of R-Type1 is predicted well by the simulation. The damage process starts at the inner rotor corners and evolves diagonally to the edge of the outer circle.

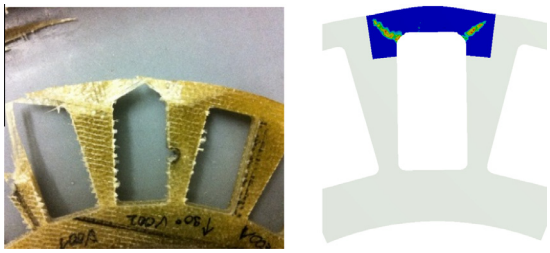

Fig. 17. Structure R-Type1: Experimental fracture pattern (left) and simulative damage evolution (right).

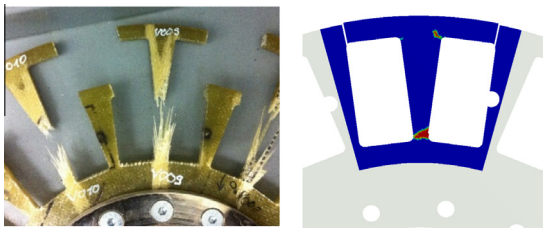

Fig. 18. Structure R-Type2: Experimental fracture pattern (left) and simulative damage evolution (right).

The damage in the R-Type2 simulation localises at the narrow transition from the inner circle to the radial bar. This explains the sudden force drop after fracture of the transition. On the other hand the experimental fracture pattern reveals that damage rather evolves radial within the bar, instead of only localizing at the root of the bar. This explains the gradual force degradation in the force displacement diagram.

6. Conclusion

This work shows, that implementing a simple CDM model into FEM simulation not only permits the realistic calculation of notched laminate strengths, but also to simulate more complex structures reasonably. The behaviour of quasi UD GF-EP is examined experimentally. In longitudinal tension, compression and transverse compression linear elastic behaviour is observed. The material behaviour in transverse tension and shear loading is nonlinear. In both cases a yield point is followed by hardening which can be regarded as linear. The material is characterised in a wide temperature range and in dependence of the global FVF. Tests on notched laminates show that the quasi UD GF-EP is rather notch insensitive, in some cases the true specimen strength even exceeded those of unnotched laminates, which is referred to as notch paradoxon. The strength prediction of open hole UD and MD laminates by means of the FEM is examined comprehensively. The key findings of this work are presented in the following:

(1) The comparison of simulations and experiments clearly shows that complete a stiffness reduction after element failure, indicated by a modified Hashin criterion, underestimates the specimen strength. Incorporating hardening can lift the calculated strength moderately; still it remains below the measured strength. To calculate realistic values it is mandatory to include the material failure process by CDM into FEM simulations. Additional incorporation of hardening alters the stress strain curve in cases where hardening is observable on specimen level. The Adjustment of the specimen strength is moderate. Fracture toughness turns out to be the decisive parameter in terms of notched laminate strength simulation.

(2) A new approach is presented to determine the fracture toughness values for the four failure modes fibre/matrix tension/compression. Laborious fracture toughness tests are avoided. Instead ordinary tension/compression tests on notched UD laminates are used in combination with a multi-target analysis to calibrate the fracture toughness values. The values determined in this manner are used in the simulation of MD laminates. The calculated specimen strengths reasonably agree with experiments, which

indicates that the calibration approach is capable of determining useful fracture toughness values. This is emphasised by the simulation of an E-Machine rotor structure.

(3) The fracture toughness values derived from RT tests are also applied to simulate longitudinal loading of notched laminates at the epoxy's rubber temperature (160 °C). The stress strain curves agree well. Thus it follows that the fracture toughness in this case is not determined by the temperature sensitive matrix but rather by the fibres.

The presented method to calibrate fracture toughness values and their insensitivity to high temperatures contribute to use the benefits of quasi UD GF-EP fabric (cost efficiency and notch insensitivity) and FRP in general in structural application.

Acknowledgement

This work was supported by the Robert Bosch GmbH in terms of a research grant and testing equipment.

References

[1] Lässig R, Eisenhut M, Mathias A, Schulte RT, Peters F, Kühmann T, et al. Serienproduktion von hochfesten Faserverbundbauteilen. Roland Berger Strategy Consultants 2012.
[2] Puck A. Festigkeitsanalyse von Faser-Matrix-Laminaten: Modelle für die Praxis. Hanser; 1996.
[3] Schürmann H. Konstruieren mit Faser-Kunststoff-Verbunden. 2nd ed. Berlin, Heidelberg: Springer-Verlag; 2007.
[4] Karahan M, Karahan N. Influence of weaving structure and hybridization on the tensile properties of woven carbon-epoxy composites. J Reinf Plast Compos 2014;33(2):212–22.
[5] Roy AK. Comparison of in situs damage assessment in unbalanced fabric composite and model laminate of planar (one-dirctional) crimping. Compos Sci Technol 1998;58:1793–801.
[6] Lomov SV, Ivanov DS, Truong TC, Verpoest I, Baudry F, Vanden Bosche K, et al. Experimental methology of study of damage initiation development in textile composites in uniaxial tensile test. Compos Sci Technol 2008;68:2340–9.
[7] Bonnafous C, Toucard F, Chocinski-Arnault L (eds.). Damage mechanisms in hemp-fibre woven fabric composites studied by acoustic emission; 2010.
[8] Daggumati S, de Baere I, van Paepegem W, Degrieck J, Xu J, Lomov SV, et al. Local damage in a 5-harness satin weave composite under static tension: Part I-Experimental analysis. Compos Sci Technol 2010;70(13):1926–33.
[9] Kergomard YD, Renard J, Thionnet A, Landry C. Intralaminar and interlaminar damage in quasi-unidirectional stratified composite structures: experimental analysis. Compos Sci Technol 2010;70(10):1504–12.
[10] Kersani M, Lomov SV, van Vuure AW, Bouabdallah A, Verpoest I. Damage in flax/epoxy quasi-unidirectional woven laminates under quasi-static tension. J Compos Mater 2015;49(4):403–13.
[11] Talreja R, Singh CV. Damage and failure of composite materials. Cambridge University Press; 2012.
[12] Aboudi J, Arnold SM, Bednarcyk BA. Micromechanics of composite materials: a generalized multiscale analysis approach. 1st ed. Amsterdam: Elsevier; 2013.
[13] Maimi P, Camanho PP, Mayugo JA, Dávila CG. A continuum damage model for composite laminates: Part I-Constitutive Model. Mech Mater 2007;39(10):897–908.
[14] Hashin Z. Failure criteria for unidirectional fiber composites. J Appl Mech 1980;47(2):329–34.
[15] O'Higgins RM, McCarthy MA, McCarthy CT. Comparison of open hole tension characteristics of high strength glass and carbon fibre-reinforced composite materials. Compos Sci Technol 2008;68(13):2770–8.
[16] Mollenhauer D, Iarve EV, Kim R, Langley B. Examination of ply cracking in composite laminates with open holes: a moiré interferometric and numerical study. Compos A Appl Sci Manuf 2006;37(2):282–94.
[17] Pinho ST, Darvizeh R, Robinson P, Schuecker C, Camanho PP. Material and structural response of polymer-matrix fibre-reinforced composites. J Compos Mater 2012;46 (19-20):2313-41.
[18] Waddoups ME, Eisenmann JR, Kaminski BE. Macroscopic fracture mechanics of advanced composite materials. J Compos Mater 1971;5(4):446–54.
[19] Whitney JM, Nuismer R. Stress fracture criteria for laminated composites containing stress concentrations. J Compos Mater 1974;8(3):253–65.
[20] Belmonte H, Manger C, Ogin S, Smith P, Lewin R. Characterisation and modelling of the notched tensile fracture of woven quasi-isotropic GFRP laminates. Compos Sci Technol 2001;61(4):585–97.
[21] Camanho PP, Maimí P, Dávila CG. Prediction of size effects in notched laminates using continuum damage mechanics. Compos Sci Technol 2007;67 (13):2715–27.
[22] Belmonte H, Ogin S, Smith P, Lewin R. A physically-based model for the notched strength of woven quasi-isotropic CFRP laminates. Compos A Appl Sci Manuf 2004;35(7):763–78.
[23] Kennedy CR, Ó Brádaigh CM, Leen SN. A multiaxial fatigue damage model for fibre reinforced polymer composites. Compos Struct 2013;106:201–10.
[24] Krüger H. Ein physikalisch basiertes Ermüdungsschädigungsmodell zur Degradationsberechnung von Faser-Kunststoff-Verbunden (Dissertation); 2012.
[25] Harris B, Engineering composite materials. IoM; 1999.
[26] Pinoh ST, Modelling failure of laminated composites using physically-based failure models; 2005.
[27] Hillerborg A, Modéer M, Petersson P. Analysis of crack formation and crack growth in concrete by means of fracture mechanics and finite elements. Cem Concr Res 1976;6(6):773–81.
[28] Jacobsen TK, Sørensen BF. Mode I intra-laminar crack growth in composites-modelling of R-curves from measured bridging laws. Compos Part A 2001;32 (1):1–11.
[29] Gregory JR, Spearing SM. A fiber bridging model for fatigue delamination in composite materials. Acta Mater 2004;52(19):5439–502.
[30] Sanford RJ, Stonesifeia FR. Fracture toughness measurements in unidirectional glass-reinforced-plastics. J Compos Mater 1971;5(2):241–5.
[31] Bažant ZP, Oh BH. Crack band theory for fracture of concrete. Mater Constr 1983;16(3):155–77.
[32] Matzenmiller A, Lubliner J, Taylor RL. A constitutive model for anisotropic damage in fiber-composites. Mech Mater 1995;20(2):125–52.
[33] Wei W. Static tensile properties simulation of plane woven-reinforced laminates with hole damage. AMR 2014;936:2017–23.
[34] Shokrieh MM, Lessard LB. Progressive fatigue damage modeling of composite materials, part I: modeling. J Compos Mater 2000;34(13):1056–80.
[35] Maimi P, Camanho PP, Mayugo JA, Dávila CG. A continuum damage model for composite laminates: Part II–Computational implementation and validation. Mech Mater 2007;39(10):909–19.
[36] Ansys Inc. (ed.). Ansys 15.0 Help: 3.22. Material Damage; 2014.
[37] Lee J, Soutis C, Measuring the notched compressive strength of composite laminates: Specimen size effects. Deformation and Fracture of Composites: Analytical, Numerical and Experimental Techniques, with regular papers 2008;68(12):2359–66.
[38] Zobeiry N, Vaziri R, Poursartip A. Characterization of strain-softening behavior and failure mechanisms of composites under tension and compression. Compos A Appl Sci Manuf 2015;68:29–41.
[39] Bergan A, Dávila C, Leone F, Awerbuch J, Tan T-M. A Mode I cohesive law characterization procedure for through-the-thickness crack propagation in composite laminates. Compos B Eng 2016;94:338–49.
[40] Ortega A, Maimí P, González E, Trias D. Characterization of the translaminar fracture Cohesive Law. Compos Part A 2016.
[41] Maimí P, Trias D, González E, Renart J. Nominal strength of quasi-brittle open hole specimens. Compos Sci Technol 2012;72:1203–8.
[42] Martín-Santos E, Maimí P, González E, Cruz P. A continuum constitutive model for the simulation of fabric-reinforced composites. Compos Struct 2014;111:122–9.